Metal Oxide Film for Growing Vertically Aligned Single-Walled Carbon Nanotubes

2009 Jpn. J. Appl. Phys. 48 085502

(http://iopscience.iop.org/1347-4065/48/8R/085502)

Metal Oxide Film for Growing Vertically Aligned Single-Walled Carbon Nanotubes

Wen-Shou Tseng, Wei-Hsiang Wang, Tasi-Hau Hong, and Cheng-Tzu Kuo[1]*

Department of Materials Science and Engineering, National Chiao Tung University, Hsinchu 300, Taiwan
[1]*Department of Materials Science and Engineering, MingDao University, Changhua 523, Taiwan*

Received December 28, 2008; revised May 1, 2009; accepted May 22, 2009; published online August 20, 2009

In the present study, we use a method that uses the oxidation state of platinum in Co–Cr–Pt oxide films to cause a volume expansion to form isolated nanoparticles through exposure to H_2 microwave plasma. The generated nanoparticles are then used to grow single-walled carbon nanotubes (SWCNTs) at ~600 °C without the application of a buffer layer using a microwave plasma chemical vapor deposition system. The effects of metal oxide film thickness on the growth of SWCNTs are investigated. The characterization techniques including X-ray photoelectron spectroscopy, scanning electron microscopy, and transmission electron microscopy are carried out, with the results showing that this method used is highly efficient in generating very small and dense catalytic nanoparticles. The results also show that, when the metal oxide film thickness is no more than 2 nm, the nanoparticles produced with diameters ranging from 2 to 3 nm can be effective for growing vertically and densely aligned SWCNTs.

DOI: 10.1143/JJAP.48.085502

1. Introduction

Recently, single-walled carbon nanotubes (SWCNTs) have been recognized as highly promising materials for a wide range of applications.[1–6] For many practical uses, vertically aligned SWCNTs are often required to be selectively grown on patterned blocks of metallic catalyst films deposited on a substrate.[7] To date, many studies have demonstrated the effective synthesis of SWCNTs.[8–11] However, except for the positive results in production scale, most processes still cannot precisely control the growth structure of SWCNTs because the growth mechanism of SWCNTs is still not well understood.

At present, catalytically supported chemical vapor deposition (CVD) is one of the most commonly used methods and is considered the best solution for nanoscale device fabrication because it not only allows a scalable process but also enables selective growth on patterned catalyst films.[12] The formation of SWCNTs using CVD involves the formation of small catalyst nanoparticles, the decomposition of hydrocarbon gases such as CH_4 and C_2H_2, and the growth of SWCNTs on the metal catalysts based on a number of diffusion models which have been proposed to explain the growth mechanism.[13,14] In one proposed model, carbon species are decomposed on the surface of metallic particles, diffuse into the particles, and are then precipitated onto the particle surface.[13] Therefore, the size of the particles is very important for the fabrication of SWCNTs.[13] Normally, catalyst particles are reduced by CVD using hydrogen plasma to form well-distributed and active metallic nanoparticles. However, this high-temperature process can induce the formation of metal silicide and the agglomeration of nanoparticles, which are unfavorable for the fabrication of SWCNTs.[14] Depositing a buffer layer between the catalyst layer and the substrate is a common way of avoiding these coarsening and impurity issues.[14–16] However, the intermediate layer itself can cause other problems, such as conductivity and adhesion issues. In addition, this layer is regarded as an impurity for many device applications. Therefore, it would be preferable to reduce the process temperature and avoid the use of a buffer layer.

It has been predicted by a previous study that very small catalytic nanoparticles less than 2 nm in diameter are required for the nucleation of SWCNTs.[17] Catalyst film thickness is very important in deciding the catalyst size when the film is converted to isolated nanoparticles by plasma treatment. As a result, regulating the catalyst film thickness should yield different carbon nanostructures. Hofmann *et al.* suggest that a reduction in Fe/Co catalyst film thickness causes a carbon nanostructure transition from larger-diameter bamboo like carbon nanofibers to smaller-diameter multi walled nanotubes with two to five walls.[18] Other studies have produced SWCNTs with entangled structures when using Co as a catalyst and with a variation in the film thickness of approximately 0.1 nm.[19]

The results of previous studies through the direct observation of the growth of SWCNTs on catalysts suggest that the formation of SWCNTs should be at a temperature of about 615 °C or even higher.[20,21] However, a very high process temperature may destroy the material and induce the formation of metal silicide, as previously mentioned. Thus, the addition of an inter layer is required. Meanwhile, the results of many studies have also shown that the fabricated SWCNTs have randomly entangled structures.[16,22–24]

The oxidation state of platinum has been shown to be very unstable to cause a volume expansion to form very small isolated nanoparticles when treated by high-intensity laser heating.[25–27] On the basis of this idea, here we aim to deposit a Co–Cr–Pt oxide film using a physical vapor deposition (PVD) system; the oxide film is then expected to be reduced to very small well-dispersed metallic nanoparticles through exposure to high-energy hydrogen plasma generated by a microwave plasma chemical vapor deposition (MPCVD) system. Subsequently, the nanoparticles formed are used to grow vertically aligned SWCNTs without the application of a buffer layer at ~600 °C by MPCVD. In addition to PtO_x, the Cr_2O_3 present in the oxide film is used as an inhibitor to prevent grain growth and thus suppress nanoparticle coarsening.[28] Additionally, metallic cobalt is an appropriate element for dissolving carbon species so as to support the growth of SWCNTs. Because film thickness is very important for determining particle size, in order to determine the optimal layer thickness for synthesizing vertically aligned SWCNTs, Co–Cr–Pt oxide film thickness is varied from 10 to 1 nm.

*E-mail address: marine.mse92g@g2.nctu.edu.tw

2. Experimental Procedure

Co–Cr–Pt oxide films with various thicknesses ranging from 10 to 1 nm were deposited on silicon wafers using a Co–Cr–Pt alloy (57 wt % Co, 11 wt % Cr, and 32 wt % Pt) as a target in an Ar/O_2 (10 sccm/30 sccm) atmosphere in the PVD system. The oxide films were accordingly reduced in H_2 microwave plasma in the MPCVD system for 10 min (100 sccm H_2, 30 Torr working pressure, ~580 °C substrate temperature, 2.45 GHz, and 600 W microwave power) to obtain well-distributed catalytic nanoparticles. The H_2-plasma-treated specimens were then heated to ~600 °C (750 W microwave power) in a CH_4/H_2 atmosphere (5 sccm/40 sccm) under a pressure of 24 Torr for 6 min to produce carbon nanostructures.

Several characterization methods were systematically used to evaluate the process results. Scanning electron microscopy (SEM; JEOL JSM-6500F) and transmission electron microscopy (TEM; JEOL JEM-2100) were used to evaluate the morphology and structure, respectively. X-ray photoelectron spectroscopy (XPS; VG Scientific Microlab 350), a surface-sensitive technique, was performed to examine the elemental composition of the metal oxide film before and after H_2 plasma treatment. Raman spectroscopy (JOBIN YVON LabRam HR800, 632.8 nm He–Ne laser) was applied for rapid identification of the resulting carbon nanostructure.

3. Results and Discussion

In this study, we have confirmed the strong correlation between Co–Cr–Pt oxidation film thickness and the resulting structure. As shown in Fig. 1, after H_2 plasma treatment, the oxidation films, except for the film with 10 nm thickness [Fig. 1(a)], are transformed into very uniform and densely dispersed nanoparticles on the substrates. Meanwhile, the particle size of the resulting nanoparticles decreases as oxide film thickness decreases. The distribution density of the nanoparticles and their particle size and chemical composition are very important in yielding vertically aligned SWCNTs.[13,29,30] As revealed in Fig. 2, the TEM image shows the morphology of the H_2-plasma-treated oxide film with a thickness of 1 nm, indicating that the generated nanoparticles are well distributed and have diameters ranging from 2 to 3 nm. This is because the oxidation phase of platinum is very unstable and can easily be decomposed to metallic state and oxygen gas by negative hydrogen ions in a high-temperature plasma environment to cause a volume expansion in the oxide film, which results in very small nanoparticles.[25–27] Furthermore, owing to the presence of Cr_2O_3, the resulting nanoparticles can be suppressed from coarsening. The combined effect can thus form very small nanoparticles without the application of a buffer layer. However, as shown in Fig. 1(a), when film thickness increases, the effect of this method becomes less significant as the cluster effect becomes increasingly dominant, leading to very large particles.

The morphologies of the as-deposited nanostructures supported by the nanoparticles generated by oxide films with thicknesses of 10, 3, 2, and 1 nm are presented in Figs. 3(a) to 3(d), respectively. Figures 3(c) and 3(d) show that the carbon nanostructures are vertically aligned on the substrates with a height of ~60 μm. In contrast, Figs. 3(a) and 3(b) show carbon nanostructures with a spaghetti-like morphology, which is typical when the deposited Co–Cr–Pt oxide film has a thickness of more than 2 nm.

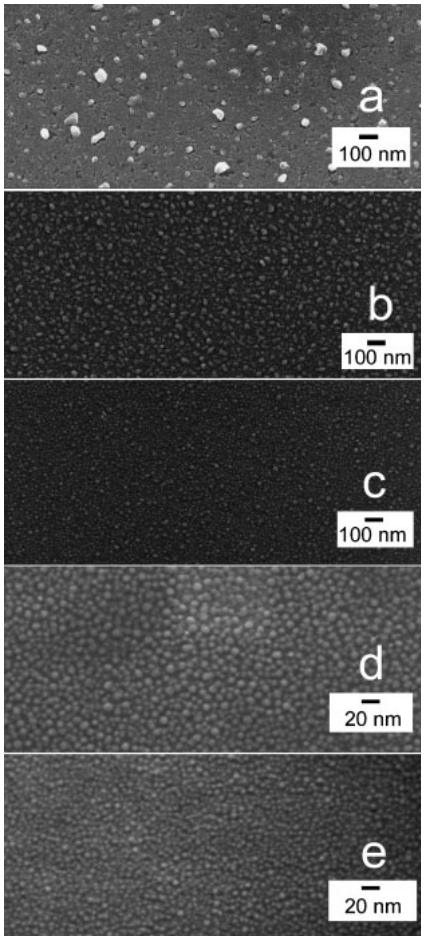

Fig. 1. SEM images of the Co–Cr–Pt oxide films on silicon wafer treated with plasma for 10 min with various thicknesses of (a) 10, (b) 5, (c) 3, (d) 2, and (e) 1 nm.

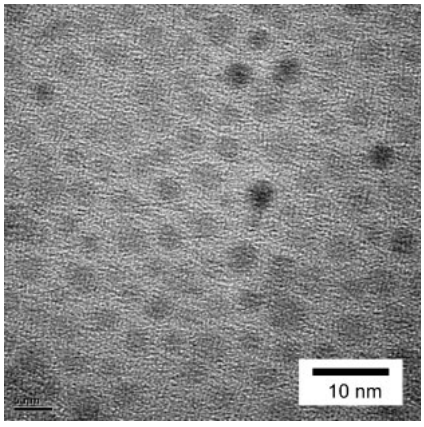

Fig. 2. TEM image of the generated nanoparticles after the oxide film (1 nm thick) was treated with H_2 plasma for 10 min.

In order to completely investigate the nanostructures, the Raman spectra of the deposited nanostructures supported by the nanoparticles generated by the metal oxide layers with various thicknesses are recorded and presented in Figs. 4 and 5. Figure 4 shows three characteristic peaks that are attributed to the D and G bands, and the radial breathing

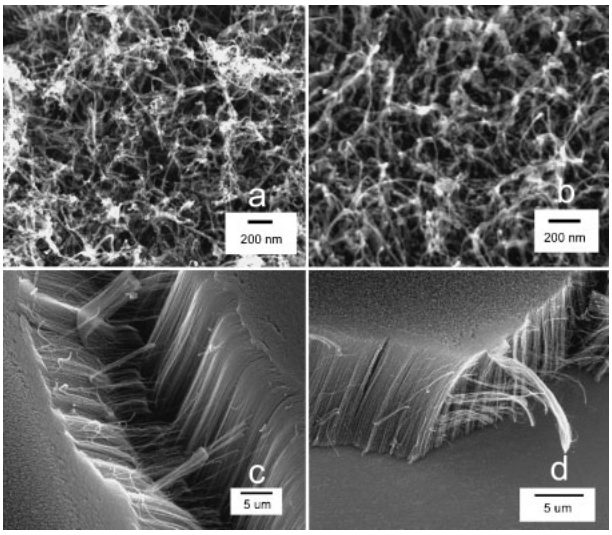

Fig. 3. SEM images of morphologies of the as-deposited nanostructures with different oxide film thicknesses: (a) 10, (b) 3, (c) 2, and (d) 1 nm.

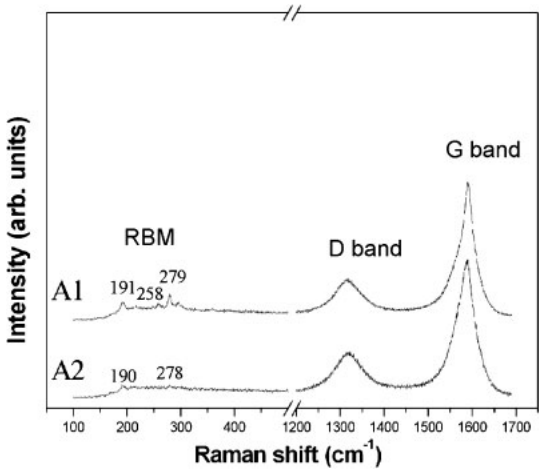

Fig. 4. Raman spectra of the as-deposited nanostructures with different oxide film thicknesses: 1 (A1) and 2 nm (A2).

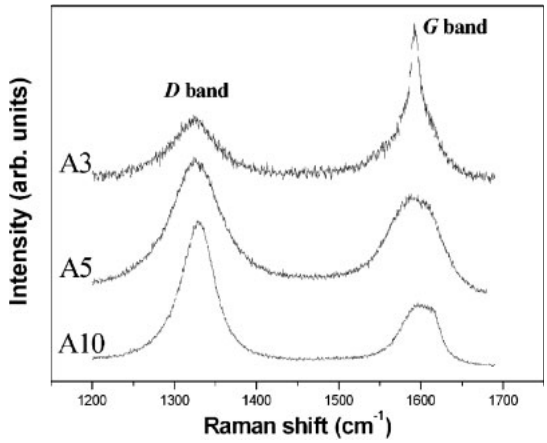

Fig. 5. Raman spectra of the as-deposited nanostructures with different Co–Cr–Pt oxide film thicknesses: 10 (A10), 5 (A5), and 3 nm (A3).

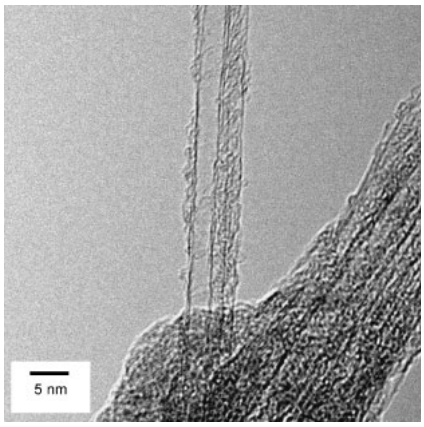

Fig. 6. TEM image of the deposited SWCNTs with Co–Cr–Pt oxide film thickness of 1 nm.

mode (RBM). By contrast, Fig. 5 only shows the spectra at frequencies from 1200 to 1700 cm^{-1} owing to the lack of an RBM signal. The intensity of the D band, at frequencies from 1300 to 1400 cm^{-1}, correlates with the structural disorder of the CNTs, which originates from defects, including disordered materials, poor graphitization, functionalized carbon, and the amorphous carbon on the sidewall of nanotubes.[31–33] The G band at frequencies from 1500 to 1600 cm^{-1} is activated by the combination of several tangential modes owing to the stretching vibrations of the CNT sidewall carbon–carbon bonds.[5,34] It is suggested that the I_D/I_G ratio is closely associated with the density of defects on the walls of the MWCNTs.[35] The RBM, located typically between 100 and 300 cm^{-1}, corresponds to the coherent vibration of carbon atoms in the radial direction, and can be a fingerprint for determining the presence of SWCNTs.[36]

The Raman scattering results show that, when the metal oxide film thickness is no more than 2 nm, SWCNTs could be grown with a low defect density. In addition, as shown in Fig. 4, it is also observed that the I_D/I_G ratio decreases from 0.27 to 0.25 as film thickness decreases from 2 to 1 nm. By contrast, MWCNTs are grown when the film thickness is larger than 2 nm. As shown in Fig. 6, the TEM image reveals that most of the SWCNTs are in the form of tube bundles. The isolated SWCNTs also have diameters of between 3 and 5 nm. However, the observation result cannot be used to precisely predict the actual distribution of nanotube diameters owing to sampling limitations.

In order to evaluate the chemical composition change of the oxide film induced by H_2 plasma treatment, the XPS profiles of each element are recorded and presented in Figs. 7–9. The Pt 4f XPS profiles are presented in Fig. 7. The Pt $4f_{7/2}$ profiles are separated into three components with binding energies (BEs) of 72.25, 73.9, and 74.6 eV. The Gauss fraction is constrained to 0.5 for all peaks. Meanwhile, the spin–orbit coupling of 3.3 eV[37,38] and the Pt $4f_{7/2}$ to Pt $4f_{5/2}$ peak area ratio of ~1.33 are consistent with theoretical values and previous reports.[37] The peak at 72.25 eV can be assigned to zero-valent platinum after the oxide film is treated with the plasma, although a previous study assigned this peak to be in the range of 71.0 to 71.3 eV.[39] This discrepancy may be due to the very small size of the Pt nanoparticles.[40,41] Thus, the BE of the nanoparticles is blue-shifted because the number of neighboring atoms and electrons is significantly reduced. This leads to less effective core-hole screening and a greater

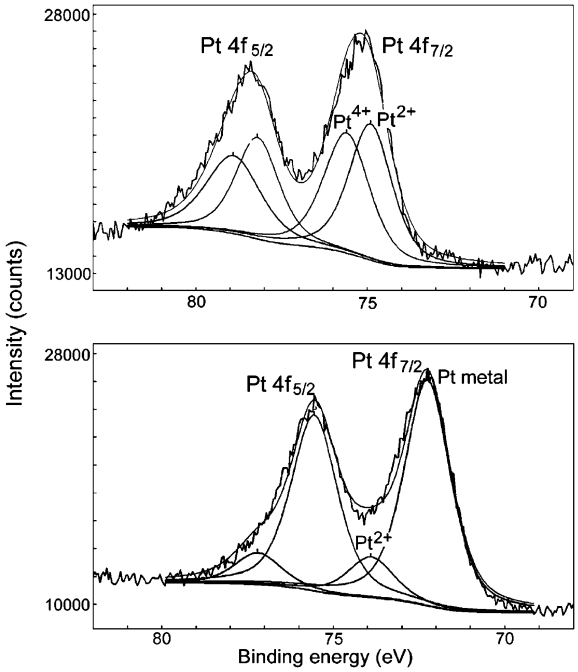

Fig. 7. Pt 4f XPS profiles of the Co–Cr–Pt oxide film (a) before H_2 plasma treatment and (b) after 10 min H_2 plasma treatment.

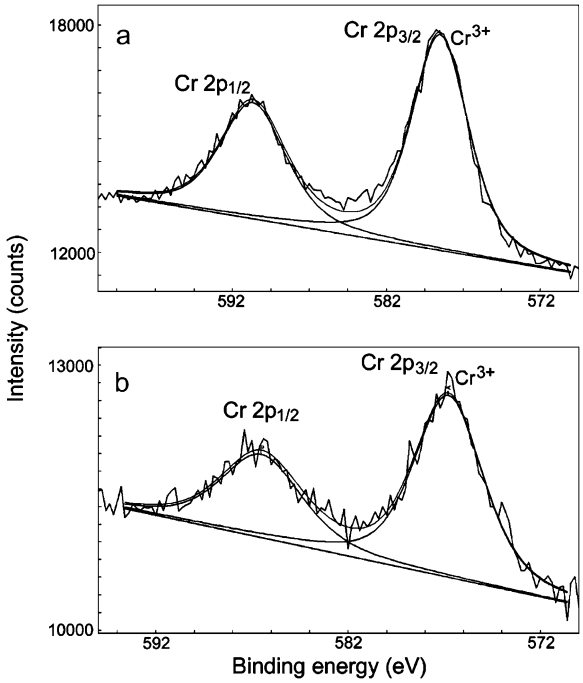

Fig. 8. Cr 2p XPS profiles of the Co–Cr–Pt oxide film (a) before H_2 plasma treatment and (b) after 10 min H_2 plasma treatment.

BE.[40] The peaks at 73.9 and 74.6 eV, corresponding to Pt^{2+} and Pt^{4+}, respectively, have also been previously reported.[39] The results show that only PtO (Pt^{2+}) and PtO_2 (Pt^{4+}) are present in the metal oxide film. It is shown that PtO_4 is eliminated after 10 min of H_2 plasma treatment. The ratio of $[Pt^{2+}]/[\text{total Pt}]$ is found to be 15%, showing that most of the platinum (~85%) has been reduced to the metallic phase.

The Cr 2p XPS profiles are presented in Fig. 8. It is shown that the Cr $2p_{3/2}$–Cr $2p_{1/2}$ spin–orbit splitting energy is approximately 9.7 eV. The Cr $2p_{3/2}$ peaks at 577.2 (prior

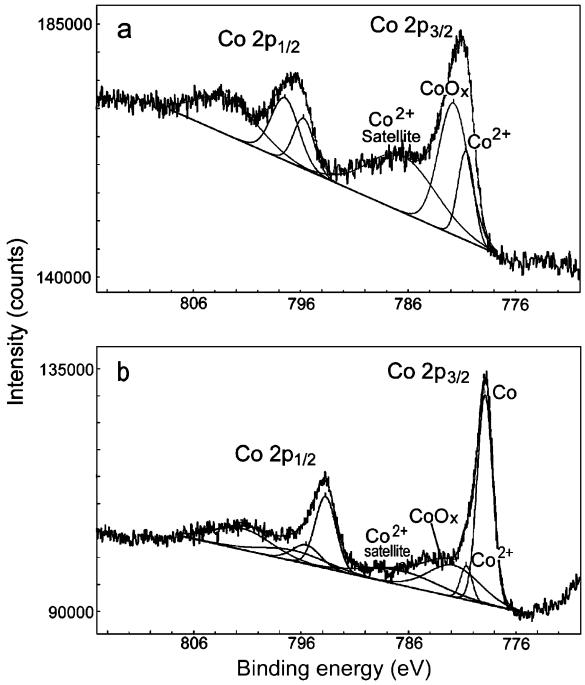

Fig. 9. Co 2p XPS profiles of the Co–Cr–Pt oxide film (a) before H_2 plasma treatment and (b) after 10 min H_2 plasma treatment.

to the plasma treatment) and 576.8 eV (after the plasma treatment) are both assigned to Cr_2O_3.[42–44] The shift of 0.4 eV may have resulted from the formation of some chromium species in the lower oxidation state on the particle surface through the decomposition of the high-oxidation-potential and high-temperature hydrogen anions in H_2 plasma. However, most of the Cr_2O_3 still plays the role of a grain growth inhibitor.

Figure 9 shows the Co 2p XPS profiles. As shown in the figure, in addition to two-spin orbital components with a spin–orbit splitting energy of approximately 15 eV, two satellite peaks can also be observed in the Co 2p core level at 786.6 (Cr $2p_{3/2}$) and ~802 (Cr $2p_{1/2}$) eV. Prior to the plasma treatment, the main structure of the Co $2p_{3/2}$ signal can be fitted into two components of 780.6 and 781.75 eV with relative intensities of 26.5 and 73.5%, respectively. The peak at 780.6 is assigned to CoO. However, it may be attributed to the Co_3O_4 spinel.[45] The peak at 781.75 eV may be due to cobalt monoxide and a mixture of oxides such as Co_3O_4. Therefore, we denote it as CoO_x. After the plasma treatment, the main peak of Co $2p_{3/2}$ is fitted to three components of 778.87, 780.6, and 781.75 eV with relative intensities of 61.9, 7.4, and 30.7%, respectively. Here, the peak at 778.87 eV is assigned to the metallic state of cobalt, although previous reports have suggested that the peak value should be between 778.1 and 778.3 eV.[39] We note that, after the treatment, the intensities of CoO and CoO_x show a significant decrease, while the intensity of the satellite peak also decreases. The characterization results reveal that, after the plasma treatment, most of the cobalt has been reduced to a metallic state so as to support the growth of SWCNTs.

All curve-fitting results above are listed in Table I. It is shown that, after the metal oxide film is treated with H_2 plasma for 10 min, high concentrations of platinum and cobalt can be effectively reduced to a metallic state, while Cr_2O_3 still remains in the nanoparticles. As suggested by Takagi

Table I. XPS profile curve-fitting results of the Co–Cr–Pt oxide film before and after the H_2 plasma treatment.

Composition element	BE (eV)	Relative intensity (%)	
		Before plasma treatment	After plasma treatment
Pt	72.25	0	84.7
PtO	73.90	51.5	15.3
PtO_2	74.60	48.5	0
Cr_2O_3	577.20 576.80	100	100
Co	778.87	0	61.9
CoO	780.60	26.5	7.4
CoO_x	781.75	73.5	30.7

et al., it is possible that Pt may not support the growth of SWCNTs in this case.[46] Therefore, the cobalt metal present in the generated nanoparticles may be the dominant element supporting the growth of SWCNTs.[19,47] Furthermore, when the as-grown SWCNT film on the Si wafer is removed and the substrate is reused to grow carbon nanostructures under the same process conditions, the fabrication results of the SWCNT film are found to be reproducible. This suggests that SWCNTs can be grown by the root-growth model.

4. Conclusions

The reduction of the Co–Cr–Pt oxide film on a silicon wafer by exposure to H_2 microwave plasma activated by MPCVD for 10 min at a temperature of ~580 °C was found to be very effective for generating very dense and small catalytic nanoparticles without the application of a buffer layer. The very small nanoparticles are formed through the reduction in the oxidation state of platinum to cause volume expansion in the oxide film in the high-energy H_2 plasma environment and the inhibition of particle grain growth with Cr_2O_3. With a high cobalt metal content, the nanoparticles are very effective for growing SWCNTs. The growth results show that, when the Co–Cr–Pt oxide film thickness is no more than 2 nm, very dense and vertically aligned SWCNTs are formed; otherwise spaghetti-like MWCNTs are fabricated.

1) B. Mahar, C. Laslau, R. Yip, and Y. Sun: IEEE Sens. J. **7** (2007) 266.
2) P. C. Collins, M. S. Arnold, and P. Avouris: Science **292** (2001) 706.
3) A. Bachtold, P. Hadley, T. Nakanishi, and C. Dekker: Science **294** (2001) 1317.
4) X. L. Liu, C. Lee, C. W. Zhou, and J. Han: Appl. Phys. Lett. **79** (2001) 3329.
5) B. J. Landi, R. P. Raffaelle, S. L. Castro, and S. G. Bailey: Prog. Photovoltaics **13** (2005) 165.
6) H. Dai: Surf. Sci. **500** (2002) 218.
7) J. I. Yeh, A. Lazareck, J. H. Kim, J. Xu, and S. Du: Biosens. Bioelectron. **23** (2007) 568.
8) M. Endo, K. Takeuchi, K. Kobori, K. Takahashi, H. W. Kroto, and A. Sarkar: Carbon **33** (1995) 873.
9) L. C. Qin, D. Zhou, A. R. Krauss, and D. M. Gruen: Appl. Phys. Lett. **72** (1998) 3437.
10) X. P. Xu and G. R. Brandes: Appl. Phys. Lett. **74** (1999) 2549.
11) E. Munoz, A. M. Benito, L. C. Estepa, J. Fernandez, Y. Maniette, M. T. Martinez, and G. F. de la Fuente: Carbon **36** (1998) 525.
12) V. B. Golovko, H. W. Li, B. Kleinsorge, S. Hofmann, J. Geng, M. Cantoro, Z. Yang, D. A. Jefferson, B. F. G. Johnson, W. T. S. Huck, and J. Robertson: Nanotechnology **16** (2005) 1636.
13) Y. Y. Wei, G. Eres, V. I. Merkulov, and D. H. Lowndes: Appl. Phys. Lett. **78** (2001) 1394.
14) T. de los Arcos, M. G. Garnier, J. W. Seo, P. Oelhafen, V. Thommen, and D. Mathys: J. Phys. Chem. B **108** (2004) 7728.
15) T. de los Arcos, P. Oelhafen, V. Thommen, and D. Mathys: J. Phys. Chem. C **111** (2007) 16392.
16) T. de los Arcos, M. G. Garnier, P. Oelhafen, D. Mathys, J. W. Seo, C. Domingo, J. V. Garci-Ramos, and S. Sanchez-Cortes: Carbon **42** (2004) 187.
17) A. Q. Jiang, N. Awasthi, A. N. Kolmogorov, W. Setyawan, A. Borjesson, K. Bolton, A. R. Harutyunyan, and S. Curtarolo: Phys. Rev. B **75** (2007) 205426.
18) S. Hofmann, M. Cantoro, B. Kleinsorge, C. Casiraghi, A. Parvez, J. Robertson, and C. Ducati: J. Appl. Phys. **98** (2005) 034308.
19) S. Noda, Y. Tsuji, Y. Murakami, and S. Maruyama: Appl. Phys. Lett. **86** (2005) 173106.
20) M. Lin, J. P. Y. Tan, C. Boothroyd, K. P. Loh, E. S. Tok, and Y. L. Foo: Nano Lett. **6** (2006) 449.
21) S. Hofmann, R. Sharma, C. Ducati, G. Du, C. Mattevi, C. Cepek, M. Cantoro, S. Pisana, A. Parvez, F. Cervantes-Sodi, A. C. Ferrari, R. Dunin-Borkowski, S. Lizzit, L. Petaccia, A. Goldoni, and J. Robertson: Nano Lett. **7** (2007) 602.
22) J. Kong, A. M. Cassell, and H. J. Dai: Chem. Phys. Lett. **292** (1998) 567.
23) L. Delzeit, B. Chen, A. Cassell, R. Stevens, C. Nguyen, and M. Meyyappan: Chem. Phys. Lett. **348** (2001) 368.
24) R. Seidel, G. S. Duesberg, E. Unger, A. P. Graham, M. Liebau, and F. Kreupl: J. Phys. Chem. B **108** (2004) 1888.
25) J. Kim, I. Hwang, D. Yoon, I. Park, D. Shin, T. Kikukawa, T. Shima, and J. Tominaga: Appl. Phys. Lett. **83** (2003) 1701.
26) T. Kikukawa, T. Nakano, T. Shima, and J. Tominaga: Appl. Phys. Lett. **81** (2002) 4697.
27) J. Y. Tseng, C. W. Cheng, S. Y. Wang, T. B. Wu, K. Y. Hsieh, and R. Liu: Appl. Phys. Lett. **85** (2004) 2595.
28) M. M. Shaijumon, N. Bejoy, and S. Ramaprabhu: Appl. Surf. Sci. **242** (2005) 192.
29) G. F. Zhong, T. Iwasaki, K. Honda, Y. Furukawa, I. Ohdomari, and H. Kawarada: Jpn. J. Appl. Phys. **44** (2005) 1558.
30) C. Laurent, E. Flahaut, A. Peigney, and A. Rousset: N. J. Chem. **22** (1998) 1229.
31) T. J. Park, S. Banerjee, T. Hemraj-Benny, and S. S. Wong: J. Mater. Chem. **16** (2006) 141.
32) A. C. Dillon, M. Yudasaka, and M. S. Dresselhaus: J. Nanosci. Nanotechnol. **4** (2004) 691.
33) S. Osswald, M. Havel, and Y. Gogotsi: J. Raman Spectrosc. **38** (2007) 728.
34) M. S. Dresselhaus, G. Dresselhaus, A. Jorio, A. G. Souza, M. A. Pimenta, and R. Saito: Acc. Chem. Res. **35** (2002) 1070.
35) A. C. Ferrari and J. Robertson: Phys. Rev. B **61** (2000) 14095.
36) A. Jorio, C. Fantini, M. A. Pimenta, R. B. Capaz, G. G. Samsonidze, G. Dresselhaus, M. S. Dresselhaus, J. Jiang, N. Kobayashi, A. Gruneis, and R. Saito: Phys. Rev. B **71** (2005) 075401.
37) G. M. Bancroft, I. Adams, L. L. Coatsworth, C. D. Bennewitz, J. D. Brown, and W. D. Westwood: Anal. Chem. **47** (1975) 586.
38) K. Kuribayashi and S. Kitamura: Thin Solid Films **400** (2001) 160.
39) C. D. Wangner, W. M. Riggs, L. E. Davies, and J. F. Moulder: *Handbook of X-ray Photoelectron Spectroscopy* (Perkin-Elmer, Eden Prairie, MN, 1978).
40) F. J. Maldonado-Hódar, C. Moreno-Castilla, and A. F. Pérez-Cadenas: Appl. Catal. B **54** (2004) 217.
41) G. C. Torres, E. L. Jablonski, G. T. Baronetti, A. A. Castro, S. R. deMiguel, O. A. Scelza, M. D. Blanco, M. A. P. Jiménez, and J. L. G. Fierro: Appl. Catal. A **161** (1997) 213.
42) P. G. Harrison, N. C. Lloyd, W. Daniell, I. K. Ball, C. Bailey, and W. Azelee: Chem. Mater. **12** (2000) 3113.
43) E. Benko, A. Wyczesany, A. Bernasik, T. L. Barr, and E. Hoope: Ceram. Int. **26** (2000) 545.
44) B. Liu and M. Terano: J. Mol. Catal. A **172** (2001) 227.
45) M. A. Langell, M. D. Anderson, G. A. Carson, L. Peng, and S. Smith: Phys. Rev. B **59** (1999) 4791.
46) D. Takagi, Y. Homma, H. Hibino, S. Suzuki, and Y. Kobayashi: Nano Lett. **6** (2006) 2642.
47) I. Wako, T. Chokan, D. Takagi, S. Chiashi, and Y. Homma: Chem. Phys. Lett. **449** (2007) 309.